Materials Today Bio 23 (2023) 100876

Contents lists available at ScienceDirect

Materials Today Bio

journal homepage: www.journals.elsevier.com/materials-today-bio

Cold atmospheric plasma-enabled platelet vesicle incorporated iron oxide nano-propellers for thrombolysis

Pei-Ru Jheng [a,1], Chia-Che Chiang [a,1], Jiunn-Horng Kang [a,b,1], Yu-Jui Fan [a,1], Kevin C.-W. Wu [c,d], Yan-Ting Chen [a], Jia-Wei Liang [a], Nima Bolouki [e], Jyh-Wei Lee [f,g], Jang-Hsing Hsieh [f,g], Er-Yuan Chuang [a,h,*]

[a] Graduate Institute of Nanomedicine and Medical Engineering, Graduate Institute of Biomedical Materials and Tissue Engineering, Institute of Biomedical Optomechatronics, International Ph.D. Program in Biomedical Engineering, School of Biomedical Engineering, College of Biomedical Engineering, Professional Master Program in Artificial Intelligence in Medicine, College of Medicine, Taipei Medical University, Taipei, 11031, Taiwan
[b] Department of Physical Medicine and Rehabilitation, Taipei Medical University Hospital, Taipei, Taiwan
[c] Institute of Biomedical Engineering & Nanomedicine, National Health Research Institute, Keyan Road, Zhunan, Miaoli City, 350, Taiwan
[d] Department of Chemical Engineering, National Taiwan University, No.1, Sec. 4 Roosevelt Rd, Taipei, 10617, Taiwan
[e] Department of Plasma Physics and Technology, Faculty of Science, Masaryk University, Brno, Czech Republic
[f] Center for Plasma and Thin Film Technologies, Ming Chi University of Technology, New Taipei City, Taiwan
[g] Department of Materials Engineering, Ming Chi University of Technology, New Taipei City, Taiwan
[h] Cell Physiology and Molecular Image Research Center, Taipei Medical University-Wan Fang Hospital, Taipei, 11696, Taiwan

ARTICLE INFO

Keywords:
Cold atmospheric plasma
Iron oxide
Platelet vesicle
Phototherapy
Magnetotherapy
Thrombolysis

ABSTRACT

A new approach to treating vascular blockages has been developed to overcome the limitations of current thrombolytic therapies. This approach involves biosafety and multimodal plasma-derived theranostic platelet vesicle incorporating iron oxide constructed nano-propellers platformed technology that possesses fluorescent and magnetic features and manifold thrombus targeting modes. The platform is capable of being guided and visualized remotely to specifically target thrombi, and it can be activated using near-infrared phototherapy along with an actuated magnet for magnetotherapy. In a murine model of thrombus lesion, this proposed multimodal approach showed an approximately 80 % reduction in thrombus residues. Moreover, the new strategy not only improves thrombolysis but also boosts the rate of lysis, making it a promising candidate for time-sensitive thrombolytic therapy.

1. Introduction

Blockages in blood vessels, whether partial or complete, can lead to serious conditions like stroke, heart attack, and pulmonary embolisms [1–12]. Thrombolytic medicines are commonly used to dissolve these blockages, either through catheter placement or systematic administration, but their effectiveness can be limited by low delivery efficiency and inadequate bioavailability, resulting in slow or incomplete recanalization [13–18]. Despite their benefits, there are still challenges to overcome in improving the delivery and effectiveness of these medicines [19–21].

Innovative therapies known as near-infrared (NIR)-light-arbitrated nanomedicines have shown promise in achieving effective thrombolytic outcomes. Biomedical optical technologies represent a promising and burgeoning field of application [22]. Photodynamic therapy (PDT) and photothermal therapy (PTT) have been found to be effective treatments for thrombosis while minimizing invasiveness [23,24]. However, most organic PTT/PDT agents have limitations, such as not being specific to thrombus location, weak resistance toward photobleaching, and a quick life span in the body [25,26].

Mechanical thrombolysis therapy is a prospective non-invasive opportunity for treating blood clots, utilizing the phase-transitional

* Corresponding author. Graduate Institute of Nanomedicine and Medical Engineering, Graduate Institute of Biomedical Materials and Tissue Engineering, Institute of Biomedical Optomechatronics, International Ph.D. Program in Biomedical Engineering, School of Biomedical Engineering, College of Biomedical Engineering, Professional Master Program in Artificial Intelligence in Medicine, College of Medicine, Taipei Medical University, Taipei, 11031, Taiwan.
E-mail address: eychuang@tmu.edu.tw (E.-Y. Chuang).
[1] These authors contributed equally.

https://doi.org/10.1016/j.mtbio.2023.100876
Received 1 August 2023; Received in revised form 8 October 2023; Accepted 18 November 2023
Available online 25 November 2023

biomaterial to create foams that dissolve clots by mechanical means. Nevertheless, the efficacy of this way is limited as bubbles only form on the interface of the clot [27]. Additionally, patients may be at danger of thrombus relapse after their initial incident. Therefore, it is necessary to not only develop efficient thrombolytic therapy that can accumulate in and diffuse throughout clots, but also prevent long-term clot recurrence. Precisely targeted delivering thrombolytic medications is suggested as a solution to these challenges, as it could increase bioavailability, precise delivery, and speed up lysis of clot [4,28].

Clinical therapies that utilize magnetic resonance imaging (MRI), fluorescent, or thermal, have shown promise in treating patients [29,30]. These techniques allow for accurate imagining of disease, real-time examining, and non-invasive evaluation of medication doses throughout treatment. Regardless of positive results in clinical settings, there is a lack of research on using multiple diagnostic techniques to guide thrombus therapy.

To address the lack of effective treatment options for thrombolysis, a new approach was proposed that combines mechanical and phototherapies using a meticulousness delivering approach and an innovative nano-theranostic. The study synthesized human platelet vesicle (PLTV) and iron oxide (IO) which serves as both photothermal and magnetic therapeutic substances, together with MRI tracers. Additionally, methylene blue (MB) was FDA approval photosensitizer and applied as a photodynamic therapy agent and fluorescence probe [31–33]. Photosensitizers receive light from outside source of light according to the feature of absorption and can go to state of excitation. In the state of excitation, they are able to react with biomolecular oxygen of the living organs and creates reactive oxygen species (ROS). MB exhibits the given absorbance in the range of 650–670 nm, aligning with the near-infrared (NIR) window I (600–900 nm), enabling effective activation in deeper tissues. MB is an economical photosensitizer derived from phenothiazinium and exhibits a high production rate of singlet oxygen ($\Phi\Delta \sim 0.5$) that finds wide-ranging applications, such as antibacterial treatments, toenail onychomycosis, and various cancer therapies. Moreover, studies have indicated that the combination of MB and photodynamic therapy offers a moderate therapeutic approach. Singlet oxygen is predominantly generated through the type II photochemical pathway of MB molecule upon excitation with light within the optical window of 600–900 nm [34]. Currently, there is active exploration of a promising approach known as ROS-mediated photodynamic therapy (PDT) for addressing peptide damage within fibrin biopolymers. This damage includes the disruption of polypeptide linkages, noncovalent interactions, and the N-attached biantennary glycan region, with the assistance of photosensitizers [25]. The ultimate goal is to potentially dismantle the fibrin skeleton within blood clots and thereby prevent the occurrence of secondary embolism resulting from post-phototherapeutic fragments. However, it's important to note that the effectiveness of most organic phototherapeutic molecules is currently limited due to their inability to accumulate specifically, susceptibility to photobleaching, and a short in vivo half-life. To mitigate these challenges and enhance both safety and thrombolytic efficacy, we have formulated a hypothesis. We propose that an approach utilizing biophysically-engineered nanomaterials to mediate a multiple-modality magnetotherapy plus phototherapy strategy may offer biosafety and thrombolytic effects, thus minimizing undesirable outcomes.

One of the four basic states of matter, and one of the more common types of matter in this Universe, plasma is an ionized gas. Technological progress has enabled scientists to create plasma systems at atmospheric pressure, which produce energetic electrons whereas heavy and neutral particles remain in the ambient temperature. This characteristic allows the use of cold atmospheric plasmas (CAP) in biomedical applications without causing harm to biological samples or organs. CAP has been studied for various biomedical purposes such as sterilization, cancer therapy, healing of wound, and regenerative biomedicine [35–39]. CAP is cable of creating a unique environment that can affect organs via chemical as well as physical interactions [40]. CAP can produce reactive oxygen/nitrogen species with different lifetimes, charged particles, pressure gradients, agitation force, and electromagnetic fields [40–43]. The combination of nanoformulations and CAP has shown promising medication effects against illnesses. In the prior studies, the plasma technique was employed to induce the self-assembly of a nanoformulation that exhibited colloidal stability or facilitated the sterilization of biomedical devices [39,44]. Here, we intended to investigate the biophysical mechanism of CAP in the formulation of the PLTV, IO, and MB mixture, resulting in the self-assembly plasma-enable nano-propeller (PLTV–IO–MB PENPs). By using various biochemical, analytical, and microscopic techniques, the study focused on providing indication that application upon CAP improves the functionalities of PLTV–IO–MB PENPs.

In addition, previous recent studies have reported the existence of corresponding receptors (IL-6R) and P-selectin glycoprotein ligand-1 (PSGL-1) inside/on platelet [45–47]. The PLTV–IO–MB PENPs could be constructed for targeting thrombus clots by binding to interleukin 6 (IL-6) and P-selectin, which are highly expressed at the clots [48–50]. The use of PLTV enabled the creation of thrombus-targeting nanomedicines.

The systemic administration of PLTV–IO–MB PENPs harnessed their unique dual-targeting capabilities, allowing them to accumulate precisely at the thrombosis site. This accumulation was effectively visualized using both fluorescent and MRI diagnostics. Meanwhile, the remaining PLTV–IO–MB PENPs were directed towards deep clots through remotely magnetic guidance, facilitated by an immobile magnet strategically positioned at the thrombosis site. Subsequently, NIR irradiation was applied to trigger both PDT and PTT effects. To further enhance the magnetic responsiveness of the PLTV–IO–MB PENPs, an actuated magnetic application was employed. These results culminate in remote photothrombolysis and magnetotherapy, respectively.

The study proposed a new approach to thrombolytic treatment by combining mechanical and phototherapies using a precision delivery strategy and nanotheranostic technology (Sch. 1). The synthesized PLTV–IO–MB PENPs showed the targeting effect on thrombus clots due to the potentially high expression of biomarkers IL-6 and P-selectin. The accumulation of the given PLTV–IO–MB PENPs at the thrombus site was visualized using MRI and fluorescent imaging, allowing for the spatial localization of thrombotic lesions. A static magnet was applied for guiding the remaining PLTV–IO–MB PENPs into deep thrombus clots, and irradiation of NIR was employed for inducing PDT and PTT performances for remote photothrombolysis. Moreover, the study also demonstrated that driven magnetically mechanical thrombolysis exercising a magnet actuated could further achieve the blood clots' lysis and avoid recurrence of thrombosis. The results showed that the approach could effectively achieve site-specific mechanical-photothrombolysis, prevent thrombosis recurrence, and be a promising applicant for effectual thrombolysis therapy in the near future.

2. Materials and methods

2.1. Materials

Human platelets were sourced from Innovative Research in Novi, MI [51]. Magnets are acquired from Bioman in Taipei, Taiwan. Chemicals such as MB, PBS, pyrrole, $FeCl_2{\cdot}4H_2O$, $FeCl_3{\cdot}6H_2O$, NH_4OH, protamine (Pro), and citric acid were obtained from Sigma-Aldrich in St. Louis, MO, USA. Antibodies against IL-6 and P-selectin were purchased from and GeneTex in TX, USA, and NOVUS in CO, USA, respectively. In this context, Pro is an FDA-approved biomaterial that can significantly improve drug encapsulation efficiency within the drug formulation [52]. All other chemicals used were of analytical grade. IO was synthesized using a co-precipitation chemical method [53], where $FeCl_2{\cdot}4H_2O$, $FeCl_3{\cdot}6H_2O$, and citric acid were dissolved in DI water and heated to 80 °C with subsequent addition of NH_4OH. The resulting IO was purified using a centrifuge filter (Amicon Ultra, 100 kDa) at 3500 rpm

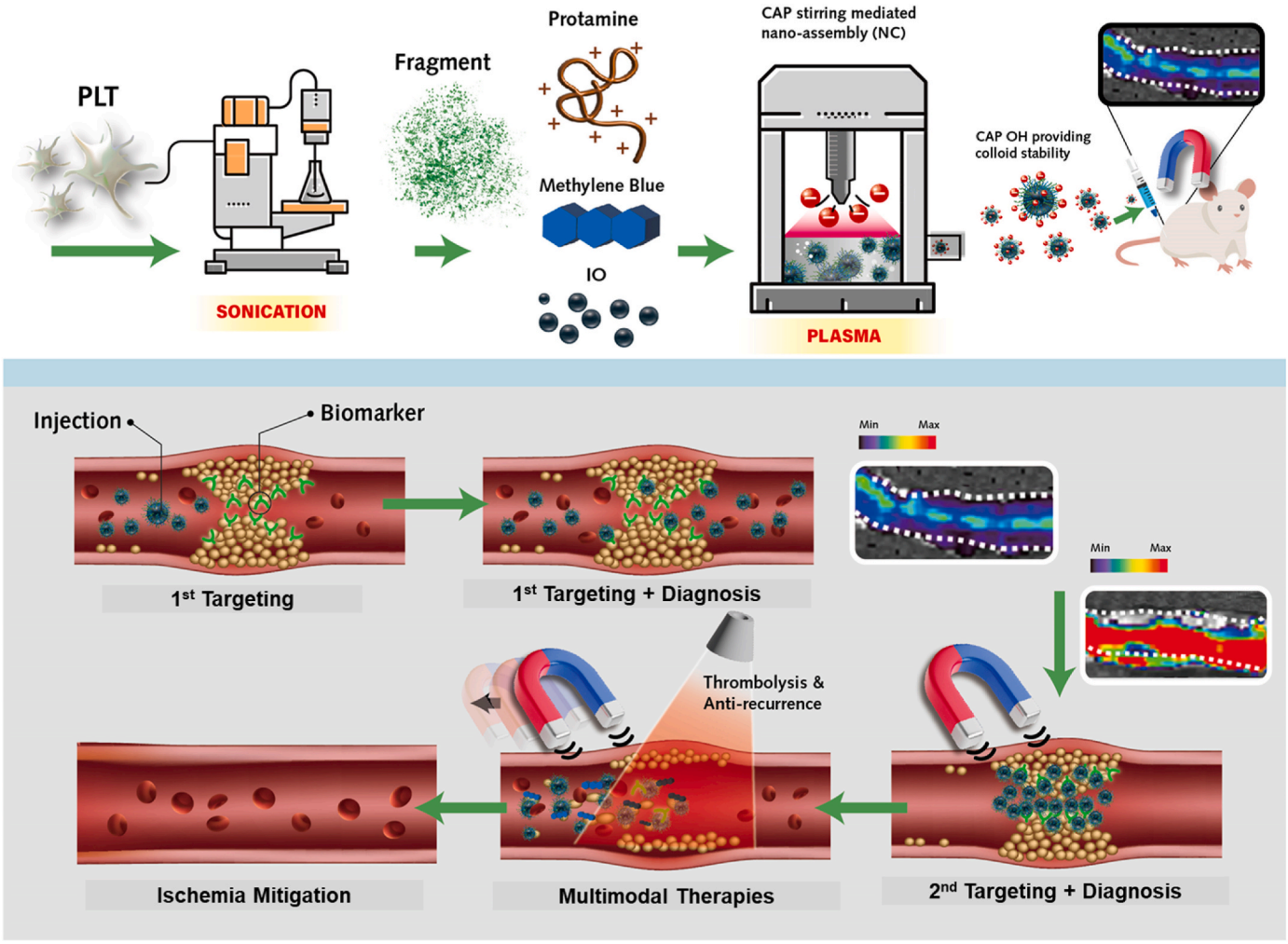

Sch. 1. The schematic illustration depicted that this study presented an innovative method for treating blood clots by combining mechanical and phototherapeutic techniques through a precise delivery approach and nano-theranostic technology.

for 20 min. Male ICR mice (6–8 weeks old) obtained from Bio-LASCO Taiwan were housed in SPF environment, and the in vivo investigations were conducted in compliance with the ethics committee of Taipei Medical University.

2.2. Cold atmospheric plasma (CAP) and PLTV–IO–MB PENPs preparation

PLTV, obtained through ultrasonication method at 4 °C for 15 min as previously described [54,55], was suspended within an PBS aqueous solution and kept in −20 °C. PLTV–IO–MB PENPs were then fabricated by means of a CAP-assisted agitating way. In this process, 0.06 mg of MB, 0.03 mg of PLTV, and 8.5 mg of IO were suspended in 9 mL of DI water having varying amounts of Pro (5, 10, 20, 50, and 100 μg/mL). The blended solution was then subjected to CAP irradiation using an extendable CAP jet that generated the reactive species for synthesizing nano-formulation in solution. The gas (argon) was utilized as the operating gas for affordability. The CAP parameters included a microsecond-pulse generator with a positive-monopolar pulse of 92 μs off-time, 8 μs on-time, and an 8 % duty cycle. A transformer amplified the microsecond (ms) pulse for supplying a given peak voltage (8 kV) for the purpose of the electrical discharge.

PLTV–IO–MB PENPs were separated by centrifugation after being subjected to CAP treatment. Centrifugation was used to remove any unencapsulated MB and impurities. The amount of unbound MB present in the supernatant was measured using UV–visible spectrophotometry at 665 nm and compared to a calibration curve method [56]. The MB encapsulating efficiency was determined employing the formula: encapsulation efficiency (%) = (mass of laden MB/MB mass in the feeding) × 100 % [57].

2.3. Optimal nano-formulation of PLTV–IO–MB PENPs and their biological, physical and chemical characteristics

The PLTV–IO–MB PENPs were analyzed for zeta potential and particle size using a Zetasizer and dynamic light scattering (DLS, Malvern Zetasizer, Nano-ZS, ZEN 3600, Worcestershire, UK), and their morphologies were studied using field-emission transmission electron microscopy (TEM, HT7700, Hitachi, Tokyo, Japan). The colloidal stability of the PLTV–IO–MB PENPs was determined by DLS measurements at 37 °C in 20 % bovine serum for 7 days, and the change in particle size at different concentrations was measured by DLS. UV–Vis absorption (EPOCH2, BioTek, VT, USA) spectra and X-ray diffraction (XRD) were used for confirming successful synthesis of the PLTV–IO–MB PENPs. The molecular weight of biomolecules was determined using SDS-polyacrylamide gel electrophoresis (PAGE) by measuring the migration distance of platelet molecules complexed by SDS.

A NIR source from Bai Qing Yuan, Taiwan was used for the photothermal evaluation, having a a wavelength range of 600–900 nm. The resultant mixture was treated by NIR for 3 min, and the temperature was determined exercising a thermal imager. The water was used as the control. The photostability of PLTV–IO–MB PENPs was also

investigated. To assess the photothermal reversibility of PLTV–IO–MB PENPs, the PENPs were irradiated with NIR for designated duration ("laser on") and then the NIR was turned off ("laser off") to allow the PLTV–IO–MB PENPs to cool naturally to room temperature. DCFH-DA (2′,7′-Dichlorodihydrofluorescein diacetate) was dissolved in ethanol, followed by adding 10 mM aqueous solution of NaOH for 0.5 h for activating the DCFH-DA. Then the as-prepared solution was diluted with PBS buffer (pH 7.4, 20 mM). The final concentration of DCFH was 40 μM. MB and PLTV–IO–MB PENPs were added into the solutions of DCFH (1.0 mL), respectively. Once saturated with oxygen, the solutions were irradiated under NIR. Fluorescence spectroscopy was used for monitoring the emission of DCF at 530 nm having the excitation wavelength of 488 nm to determine the PDT effect [58].

In vitro MB release test, PBS containing either 500 μg of PLTV–IO–MB PENPs or free MB was supplemented into a dialyzed bag with a molecular weight cutoff (MWCO) of approximately 100 KDa. The dialysis bag was then immersed in a sealed tube containing PBS with 10 % bovine serum albumin (BSA) and stirred at 150 rpm. The entire setup was incubated in a shaking incubator at 37 °C. At programmed time points, dialysate was collected and replaced with the same volume of fresh PBS. In addition, a separate NIR source was used to irradiate the PLTV–IO–MB PENPs in the dialysis bag for evaluating the photo-activated release performance of MB. The mass concentration of MB in the collected dialysates was measured using a microplate reader (EPOCH2, BioTek, VT, USA) to estimate the cumulative release of MB at different time intervals.

To determine the optimal positioning of a bar magnet for achieving a durable magnetic field and remoting magnetism of PLTV–IO–MB PENPs, an *in vitro* test was conducted to observe the motion of PLTV–IO–MB PENPs along a movement magnetic field employing a camera in a capillary tube.

Fluorescence data of MB formulations were acquired exploiting an IVIS (IVIS Spectrum, Lumina III XRMS, MA, USA) or fluorescence spectrometer. The relaxivity values (r1 and r2) of PLTV–IO–MB PENPs were measured utilizing a 7 T MRI scanner (EPOCH2, BioTek). T2 (transverse relaxation) times were measured employing a multi-echo spin-echo sequence with echo times (TE). The average T2 times were next exercised for calculating the transverse relaxivity (r2). A Superconducting Quantum Interference Device (SQUID) was employed to conduct magnetic evaluation and characterization of the PLTV–IO–MB PENPs. The components of the test samples were further characterized using field emission scanning electron microscopy equipped with an energy-dispersive X-ray spectrometry (EDS) detector.

For the purpose of *in vitro* thrombolytic evaluation, we utilized the fluorescent dye fluorescein isothiocyanate (FITC) to label and associate with fibrin clots in accordance with a previously published method [25]. FITC-conjugated fibrin clots were generated by adding 25 U/mL of thrombin and 2.5 mM of calcium peroxide to a fibrinogen solution, which contained 450 μL of 1 mg/mL fibrinogen along with 50 μL of 1 mg/mL FITC-conjugated fibrinogen. The mixture was then incubated at 37 °C for 60 min. Subsequently, the FITC-conjugated clot was exposed to various formulated groups (clot + magnet (Mag) + NIR + external magnet (Veer Mag), clot + MB + Mag + NIR + Veer Mag, clot + PLTV–IO–MB PENPs, clot + PLTV–IO–MB PENPs + NIR, clot + PLTV–IO–MB PENPs + Mag + Veer Mag, and clot + PLTV–IO–MB PENPs + Mag + NIR + Veer Mag) for 60 min and assessed using a fluorescence microscope.

2.4. Animal studies

The animals and the experimental protocol were approved by the Institutional Animal Care and Use Committee at Taipei Medical University. ICR mice were anesthetized with isoflurane (ca. 1–4%) via inhalation. After the mouse was positioned in a supine position and confined with medical adhesive tape, depilatory cream was used for removing fur. An in vivo midline incision was created along the abdomen, and the mesenteric vessels were exposed by gently separating the tissue. Filter paper (ca. 2 × 2 cm) soaked with a 35 % ferric chloride solution was then placed over the mesenteric vascular tissues for 5 min to induce vascular thrombosis. The mesenteric vessels were washed subsequently with PBS for removing any ferric chloride solution residual.

2.5. Evaluation of thrombolysis and biodistribution in vivo

To evaluate the effectiveness of PLTV–IO–MB PENPs in improving accumulation, targeting, and penetration of thrombus clots in vivo, a study was conducted using thrombus-bearing animals divided to serval groups ($n \geq 3$ per group). Mice in the first group were injected systemically with 100 μl of MB, while mice in the second group received an equivalent amount of PLTV–IO–MB PENPs with a concentration of 10 μg/mL of MB. For mice in the third group, PLTV–IO–MB PENPs were administered along with the placement of a static magnet (0.2 bar) adjacent to the thrombi for 25 min (Mag), while animals no magnet placement served as the compared experimental group. The tissues of vessels of the mice in all three groups were assessed using T2-MRI (PharmaScan) or IVIS (Lumina III XRMS) for estimating the extent of accumulation. To evaluate the photothermal effectiveness in vivo, an NIR source (3 min) was used for the treated vascular tissues, and a thermal imager was applied for measuring the vessel temperature. For assessing the expression of BMs (biomarkers), immunofluorescence and microscopic analyses were performed using fluorescence-conjugated IL-6, P-selectin, heat shock protein (HSP), CD86 (M1 macrophage), plasminogen activator inhibitor-1 (PAI-1), and CD206 (M2 macrophage) primary antibodies (1:100, 1 h, 37 °C) on thrombus and health vascular tissues. DAPI (Biotium #40043, 1:100, 23 °C, 30 min, CA, USA) was used as a counterstain for nuclei. The fluorescent extent of the immunofluorescent sections was evaluated using ImageJ software.

In the photo-treated group, an NIR source (3 min) was used for the treated vascular tissues. It is important to note that in this study, the PLTV–IO–MB PENPs developed not only have phototherapeutic properties but also were expected to have magnetically induced mechanical thrombolytic theranostic performance. In the magnet-treated group, a static magnet (Mag, 0.2 bar) was placed statically adjacent to the clots for 25 min. The magnet was next actuated along the vessel in a parallel way five times having 0.2 bar as veer magnet for magnetic thrombolysis (Veer Mag). For assessing the thrombolysis effectiveness in vivo was evaluated by administering 100 μl of PBS (Mag + NIR + Veer Mag), PLTV–IO–MB PENPs + Mag, PLTV–IO–MB PENPs + Mag + NIR, or PLTV–IO–MB PENPs + Mag + NIR + Veer Mag having an equivalent dosage of MB (10 μg/mL). After euthanizing the mice by means of CO_2, the vascular tissues were removed and harvested for hematoxylin and eosin (H&E) staining and histological microscopic analysis. The sections for histology were conducted and processed exploiting ImageJ software. The quantitative areas of in vivo thrombus clots were measured, and the efficiency of thrombolysis was determined as per the area ratio (100 %) of occlusion to the complete vasculature.

Targeted delivery and homing of nano-formulations to specific lesion sites through systemic administration is crucial for effective disease treatment. It is important to identify suitable fluorescent dyes and corresponding analogs that accurately reflect the in vivo biodistribution of drug molecules or drug carriers. Currently, nano-formulations formulated with drug-dye or polymeric-dye conjugates are considered reliable approaches for mimicking the biodistribution of nanomedicine in vivo. In this study, we employed polymeric-conjugated dyes (specifically, FITC-NHS ester) to create FITC-conjugated nano-formulation (PLTV–IO–MB PENPs), using methods previously reported [59].

To determine the in vivo distribution of fluorescent FITC-conjugated PLTV–IO–MB PENPs in mice, we administered 0.2 mL of FITC-conjugated PLTV–IO–MB PENPs and MB solutions separately into the mice. Subsequently, soft tissues (heart, liver, spleen, lung, and kidney) fluorescence images of the animals were captured at 1, 3, and 7 time

points after systemic administration, using an in vivo imaging system (IVIS). Following imaging, the treated animals were sacrificed, and major organs, including the kidneys and liver, were harvested for histological optical imaging to further analyze the distribution of the nanoformulations. In the plasma pharmacokinetic study, blood samples of MB or PLTV–IO–MB PENPs administered animals were collected in heparinized tubes both before dosing and at specific time points following administration. Plasma was promptly separated by centrifugation at 6000 rpm for 10 min and subsequently stored at −80 °C until it underwent spectrometric analysis.

In the liver bleeding assay, after the administration of MB and PLTV–IO–MB PENPs to ICR mice under anesthesia, a liver injury was induced using a 20-gauge needle to facilitate bleeding for 5 min. Subsequently, the blood was allowed to collect on filter paper, and the extent of bleeding was assessed by measuring the weight of the filter paper containing the blood.

2.6. Statistical analysis

The experimental data are presented as mean ± standard deviation (SD). Statistical analysis was performed using Kruskal-Wallis test to determine the significance of differences between groups. A p-value less than 0.0332 (*), 0.0021 (**), 0.0002 (***), or <0.0001 (****) was considered statistically significant.

3. Results and discussion

3.1. Characterization of CAP

We prepared nanoformulations consisting of MB, PLTV, and protamine cross-linkers using a CAP [44] combined with ionic gelation [60]. The CAP process (Fig. 1a) involves generation of the PLTV–IO–MB PENPs upon the CAP treatment, where energetic electrons generated during electrical discharge dissociate water molecules into radicals and

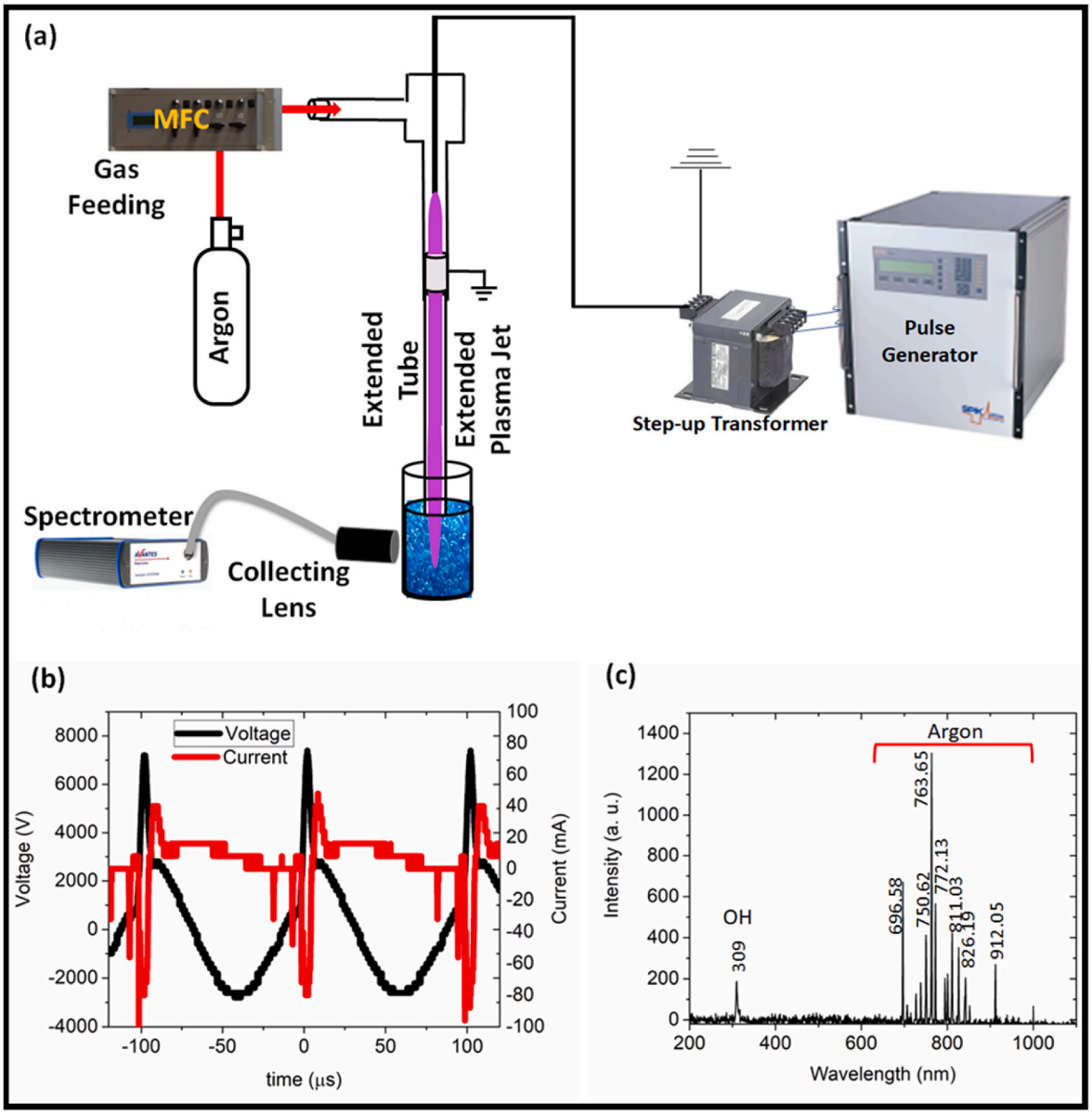

Fig. 1. CAP tests. (a) Photographic results of the cold atmospheric plasma (CAP) jet device used for nano- PLTV–IO–MB PENPs generation. It displays a picture of the CAP interacting with the nanocluster solution. For characterizing the excited and reactive species in the interaction with the mixture solution, OES was utilized, and a collecting lens was positioned downstream of the system. (b) CAP working parameter of voltage/current vs. time. (c) Optical emission spectroscopy (OES) emission spectra data, where hydroxyl radicals (309 nm) and argon-excited species were the dominant species detected.

ions for example hydroxyl. The parameters for the CAP (capacitive coupled) system included a microsecond pulse generator which produced a positive monopolar pulse with 8 μs on-time and 92 μs off-time, resulting in an 8 % duty cycle. The microsecond pulse was amplified by a step-up transformer to achieve a given peak voltage (8 kV) for the purpose of electrical discharge (Fig. 1b).

This process induces colloidal coagulation and enhances the intensity as well as probability of mutual particle collisions through stirring-induced shear. We used optical emission spectroscopy (OES) to measure the excited and reactive species generated during interactions with the nanocluster solution. OES (Fig. 1c) showed that the dominant species in the OES data seems argon-excited species and hydroxyl radicals (309 nm). The pH level of the solution was determined using a pH probe [61].

3.2. Characterization of PLTV–IO–MB PENPs

The DLS data illustrates the particle size that was obtained at varying concentrations (5, 10, 20, 50, and 100 μg/mL) of Pro in the mixture (0.06 mg MB, 0.03 mg PLTV, and 8.5 mg IO) when subjected to CAP treatment (Fig. 2a). As the concentration of Pro increases, the formed particle size also increases. Reducing the size of particles can facilitate the entrapment of higher concentrations of therapeutic agents, enhance drug stability and bioavailability, and enable sustained delivery of the medication. To achieve the optimal particle size for vascular delivery, the Pro group with a concentration of 10 μg/mL (approximately 250 nm) was selected. This size falls within the recommended limit of 300 nm or less [62]. The DLS finding displays the zeta potential measurements of Pro at different concentrations (5, 10, 20, 50, and 100 μg/mL) following CAP treatment. The results indicate that all experimental groups exhibited anionic charged properties (Fig. 2b).

The crystallinity of PLTV–IO–MB PENPs was assessed using XRD following CAP treatment, and the results were presented in Fig. 2c. The XRD patterns indicated that IO or PLTV–IO–MB PENPs displayed well-defined crystalline peaks, with IO signals being identifiable at a diffraction angle of 2θ equal to ca. 35° (311), 43° (400), 53° (422), 57° (511), and 63° (440) [63]. In contrast, PLTV exhibited a broad peak with a 2θ angle between 30° and 60°, which is indicative of an amorphous structure.

The DLS result illustrates that the PLTV–IO–MB PENPs formed by CAP had a more negative surface charge (Fig. 2d). The generation of anionic hydroxyl radicals by CAP irradiation caused a reduction in the interface charge of the CAP-made PLTV–IO–MB PENPs, as shown in the data of zeta potential (Fig. 2d). The use of CAP to create a strong interface charge and improve stability in colloidal phase could be a new approach for the synthesis of durable and functional nanoformulations. The colloidal stable property of the CAP-formed PLTV–IO–MB PENPs was verified, and it was found to be superior to that of the mixture with no treatment of CAP. The UV–vis spectra show IO (green), MB (blue), and PLTV–IO–MB PENPs (black) dispersions (Fig. 2e). The absorbance peak at around 660 nm having a peak at around 600 nm was observed in the MB spectrum of the aqueous solution. Both MB and IO have their NIR-responsive phototherapeutic significance in the NIR window of 600–900 nm. This spectrum indicates the start of visible absorption ranging 600–900 nm.

The PLTV was analyzed using SDS-PAGE (Fig. 2f), and the gel image showed that PLTV had a board biomolecular weight of approximately ranging from 10 to 240 kDa. This may be related to the cluster of IL-6 receptor and P-selectin ligand, which is likely to exist in platelets and is involved in the IL-6 and P-selectin ligand/receptor axis in cardiovascular diseases. However, there was no evidence of any degradation or alteration of the PLTV protein structure.

The mechanical agitation caused by CAP, an innovative way for breaking up mixtures of complex, led to the formation of nanoclusters during the process of CAP application. This favored the formation of heart-shaped granular nano-propellers in comparison with mechanical

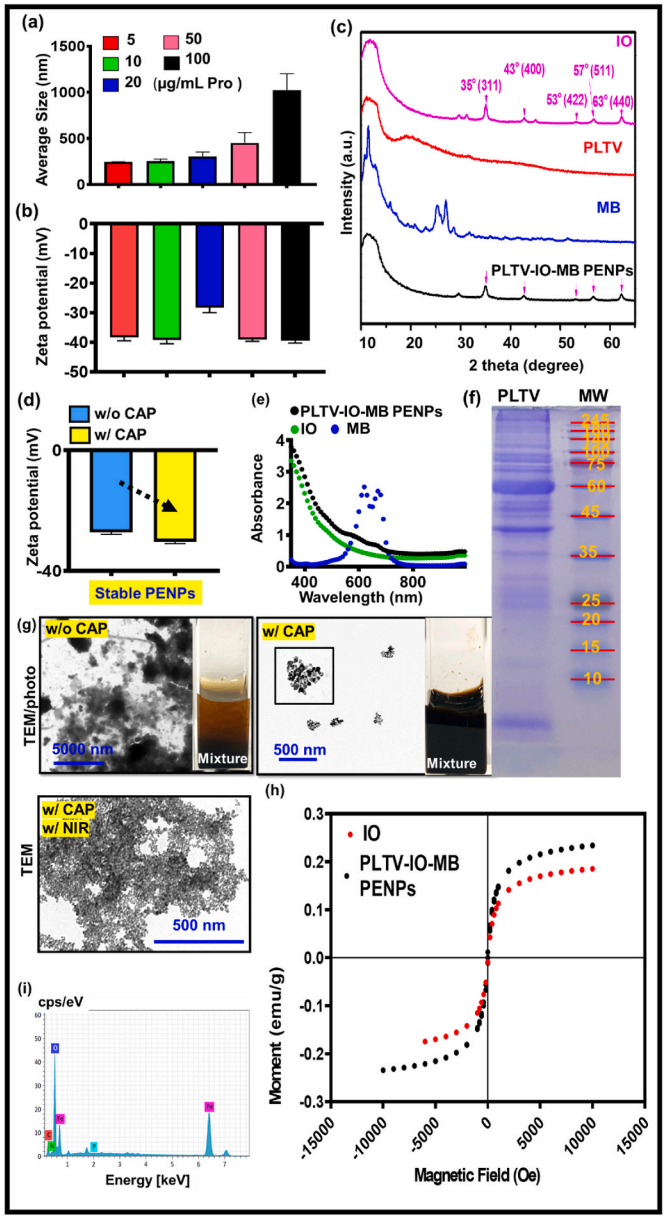

Fig. 2. Characterizations tests. (a) The particle size and (b) zeta potential test for the optimized formulation (n = 3). (c) X-ray diffraction (XRD) measurement. (d) Zeta potential measurements for colloidal stability of CAP-derived PLTV–IO–MB PENPs (n = 3). (e) UV–Vis spectra displaying absorbance of iron oxide (IO) (green), MB (blue), and PLTV–IO–MB PENPs (black) dispersion. (f) SDS-PAGE analysis of PLTVs. (g) TEM data of the mixture (MB, PLTV, Pro, and IO) with or without CAP application, or with CAP plus NIR. (h) SQUID, (i) EDS analysis of PLTV–IO–MB PENPs. (For interpretation of the references to color in this figure legend, the reader is referred to the Web version of this article.)

agitation without treatment of CAP, according to TEM data (Fig. 2g). The TEM images showed that CAP treatment (PLTV–IO–MB PENPs) resulted in more uniform particle sizes and smaller particles with low polydispersity. Conversely, no CAP, the quality of dispersion showed aggregation, large particle size, and high polydispersity, as demonstrated by both the TEM images and DLS data. When subjected to near-infrared (NIR) irradiation, the morphological structure of PLTV–IO–MB PENPs experienced significant disruption and breakage, resulting in an irregular structure. This was confirmed through the analysis of TEM data.

By analyzing the remanence shown in Fig. 2h, it was determined that

the total magnetic moment of the PLTV–IO–MB PENPs originates from the magnetic Fe component. This observation confirms that the SQUID data obtained are consistent with the magnetization measurement and provides clear evidence of the magnetic nature of the PLTV–IO–MB PENPs. The surface element distribution of the sample was investigated using EDS, as depicted in Fig. 2i. The analysis revealed the presence of O, Fe, N, P, and C elements in the PLTV–IO–MB PENPs. These results have established that the presence of O, Fe, N, P, and C elements can be primarily attributed to the PLT, MB, and IO components. Previous research has shown that protamine's cationic arginine components can form ionic bonds as well as anionic biomaterials [64]. The occurrence of CAP promotes the production of reactive oxygen species, electrically charged particles, and mechanical agitation, which work together to encourage the spontaneous creation of stable self-assembled nanoclusters. A previous study examined the impact of plasma crosslinking [65]. As per the previous finding, Poly (ethylene terephthalate) can be aminated through plasma treatment [66]. Plasma generation using noble gases creates free radicals that result in crosslinking and the formatting active sites for following chemical reactions. CAP treatment can produce shorter chains that allow for improved reorganization of starch in the crosslinking procedure, leading to improved crosslinker efficiency in following reactions [67]. Furthermore, plasma jet treatment under CAP can facilitate the crosslinking of dentin collagen, as reported in previous literature [68]. The result indicates that cross-linking of MB, PLTV, IO, and Pro occurs within application of CAP and that CAP promotes particle stability and nanoassembly (Figs. 1 and 2).

Molecular imaging using MRI is useful for detecting acute thrombosis non-invasively with high spatial resolution. To investigate the MRI properties of PLTV–IO–MB PENPs, T2* images were obtained at different concentrations. As shown in Fig. 3a, the MRI signal decreased as the concentration of PLTV–IO–MB PENPs increased, indicating a strong magnetic field gradient. The relaxation rate (R2) is assessed for rising IO amounts of PLTV–IO–MB PENPs, confirming the excellent MR features of PLTV–IO–MB PENPs. MRI data (Fig. 3a) reflected that PLTV–IO–MB PENPs can be used as an appropriate MRI diagnosis agent with homogenous signal intensity, highlighting its potential as a diagnostic tool for thrombosis.

The study evaluated the photothermal conversion ability of PLTV–IO–MB PENPs. Different concentrations of the samples were exposed to a source of NIR light for 3 min, and thermographic data were recorded (Fig. 3b). The temperature of the samples increased in a manner dependent on IO concentration and power density (Fig. 3b). Three cycles of on/off NIR laser irradiation on the PLTV–IO–MB PENPs were performed. As shown in Fig. 3c, a temperature change of ca. 10 °C of the PLTV–IO–MB PENPs was achieved once the first cycle of laser irradiation but did not show observable decrease after two additional cycles, indicating good photostability of PLTV–IO–MB PENPs. In a previous study, the photothermal effect of Fe_3O_4 nanoparticles with different shapes was investigated for cancer therapy. The study reported that red and NIR irradiations were applied for inducing the photothermal performance *in vitro* and in vivo [69].

Previous investigations have shown that once photosensitizers are laden into metal-based nanocarriers, the electron interacts with the plasmon of the nanocarrier, causing the photosensitizers to be quenched initially in delivery of drug. Only upon release to the targeted disease do the photosensitizers become bioactive [70]. For measuring the drug release *in vitro*, a free-form drug is often used as a control group [71]. A free-form MB was exercised as a control group for determining the MB's release.

The release of MB from the PLTV–IO–MB PENPs was studied by means of UV–Vis spectroscopy under neutral buffer (pH 7.4) and solution + NIR irradiation. A profile of release was obtained (Fig. 3d), where the free-form MB was rapidly released within a short period (Fig. 3d). NIR irradiation led to a significant enhancement in the release of MB from the NCs, suggesting that NIR light irradiation was highly effective

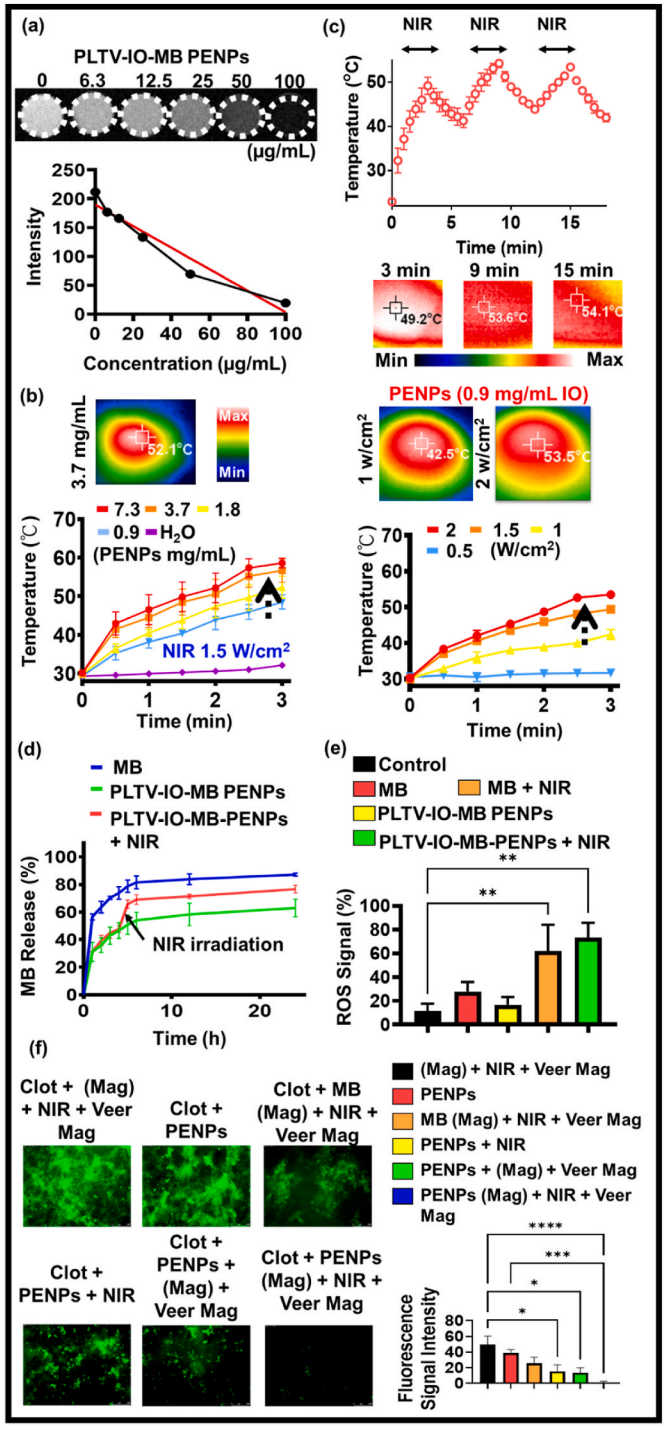

Fig. 3. Displays characterization tests that were conducted. (a) MRI results and their quantitative analysis. (b) The phototherapeutic and (c) repeatable photothermal effects of PLTV–IO–MB PENPs (n = 3). (d) The *in vitro* release profile of MB in the free-form MB or PLTV–IO–MB PENPs group (n = 3). (e) The 2′-7′-Dichlorodihydrofluorescein diacetate (DCFH-DA) assay was used to estimate the PDT effect of test samples (n = 3). (f) The *in vitro* thrombolytic assay. The experimental data are presented as mean ± standard deviation (SD).

in facilitating MB release. This NIR-induced drug release was attributed to the disturbance of noncovalent interactions that resulted from NIR-photothermal transitions (as illustrated in Fig. 3d). When photosensitizers are encapsulated within a nanocarrier, their electrons engage with the plasmon field of the nanocarrier. This interaction leads to the initial quenching of the photosensitizers during the drug delivery process. As

per prior research findings, the photosensitizer regains its activity only upon release within the target lesions [70]. Consistent with the TEM data (as shown in Fig. 2g), the *in vitro* release outcomes supported the targeted release triggered by external NIR stimulation, which could potentially minimize systemic drug bio-distribution and associated undesirable side effects.

Together with PTT once NIR-mediated irradiation driven photo-therapeutic outcomes, as PDT effect via the formation of ROS generated upon photoactivation, it is feasible for determining sensitizer concentration indirectly with assaying ROS. Accordingly, a previously described assay [72] involving the transformation under photooxidation of 2′–7′-dichlorofluorescin diacetate (DCFH-DA) into highly fluorescent 2′-7′-dichlorofluorescein (DCF) was adapted. Light irradiation of a photosensitizer causes the production of ROS that, in the presence of DCFH, lead to generation of DCF, a highly fluorescent compound that is easy to measure. The fluorescence data showed that the MB or PLTV–IO–MB PENPs upon the NIR irradiation generated considerable ROS, indicating PDT effect achievable, as per DCFH-DA assay (Fig. 3e).

Encouraged by the impressive photothermal, photodynamic, and magnetic capabilities demonstrated by PLTV–IO–MB PENPs when exposed to NIR laser irradiation and magnetic fields, we proceeded to perform an FITC-labeled fibrin clot assay. This assay provides a straightforward method for evaluating the structural disruption of fibrin networks. Significantly, in contrast to the green-fluorescent-labeled fibrin clots those subjected to various experimental conditions such as magnet (Mag) + NIR + external magnet (Veer Mag), MB + Mag + NIR + Veer Mag, PLTV–IO–MB PENPs treatment alone, PLTV–IO–MB PENPs + NIR treatment, and PLTV–IO–MB PENPs + Mag + Veer Mag treatment, we observed a substantial breakdown of the fibrin network when fibrin was co-cultured with PLTV–IO–MB PENPs and exposed to Mag + NIR + Veer Mag. This outcome suggests that the thermal energy, ROS-induced oxidation, and magnetic forces collectively contributed to the disruption

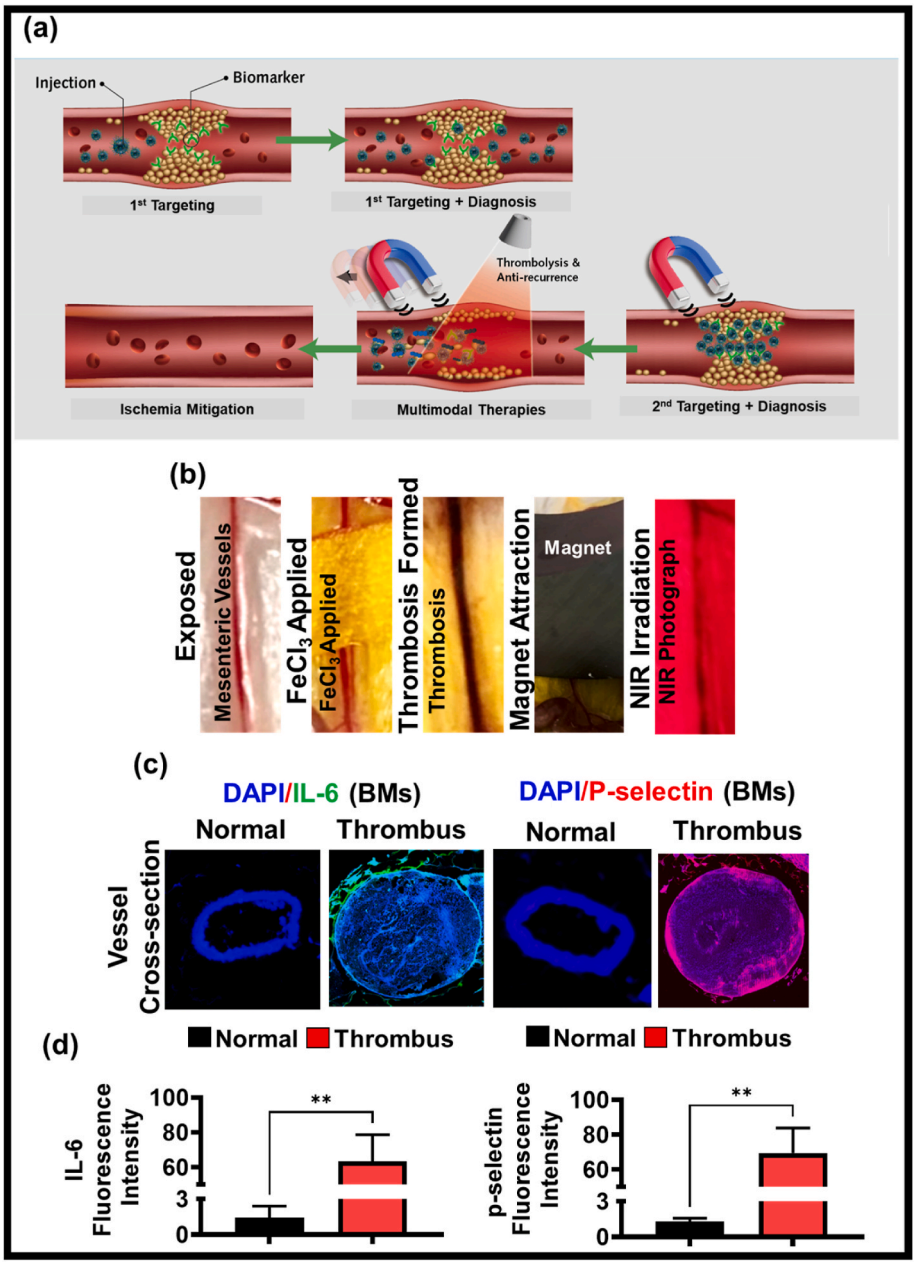

Fig. 4. The results of in vivo tests conducted in the study. (a) It depicts a schematic illustration of the targeting and theragnostic performance of PLTV–IO–MB PENPs. (b) The data presents images of the model creation, magnetic application, and NIR irradiation. (c) The finding displays microscopic data and (d) quantitative results indicating the thrombus vascular expression of IL-6 and P-selectin. The experimental data are presented as mean ± standard deviation (SD).

of the fibrin network (see Fig. 3f).

3.3. *In vivo studies using a $FeCl_3$ method induced thrombus animal model*

Thrombosis is a condition in which blood components, such as fibrin and platelets, clump together and obstruct blood vessels. This can cause serious damage to organs and tissues that rely on that blood supply, and it is a major cause of mortality and disability worldwide (almost one-third of annual mortalities) [73,74]. The schematic illustration indicates how PLTV–IO–MB PENPs can target and treat thrombosis (Fig. 4a). The photographic data shows the process of how this is done, including inducing thrombosis in an ICR mouse model with $FeCl_3$, applying a magnet, and then treating with NIR light (Fig. 4b).

IL-6 and P-selectin are two appearing biomarkers (BMs) that are precisely upregulated in thrombosis lesion or clots [48–50]. Recent studies have validated the presence of soluble IL-6R receptors and PSGL-1 on or within platelets [45–47]. This specific binding mechanism could make IL-6 and P-selectin ideal targets for PLTV–IO–MB PENPs to bind to and accumulate at the site of thrombus clots, aiding in the detection and imaging of the clot. PLTV–IO–MB PENPs can be used to monitor or enhance the effectiveness of thrombolysis. Fluorescence microscopic data demonstrated that thrombus clots had higher levels of IL-6 and P-selectin expression than healthy blood vessels (Fig. 4c and d).

3.4. *In vivo studies of multimodal diagnosis for thrombus animals after administration of PLTV–IO–MB PENPs*

The detection and thrombus lysis in vessel illnesses using

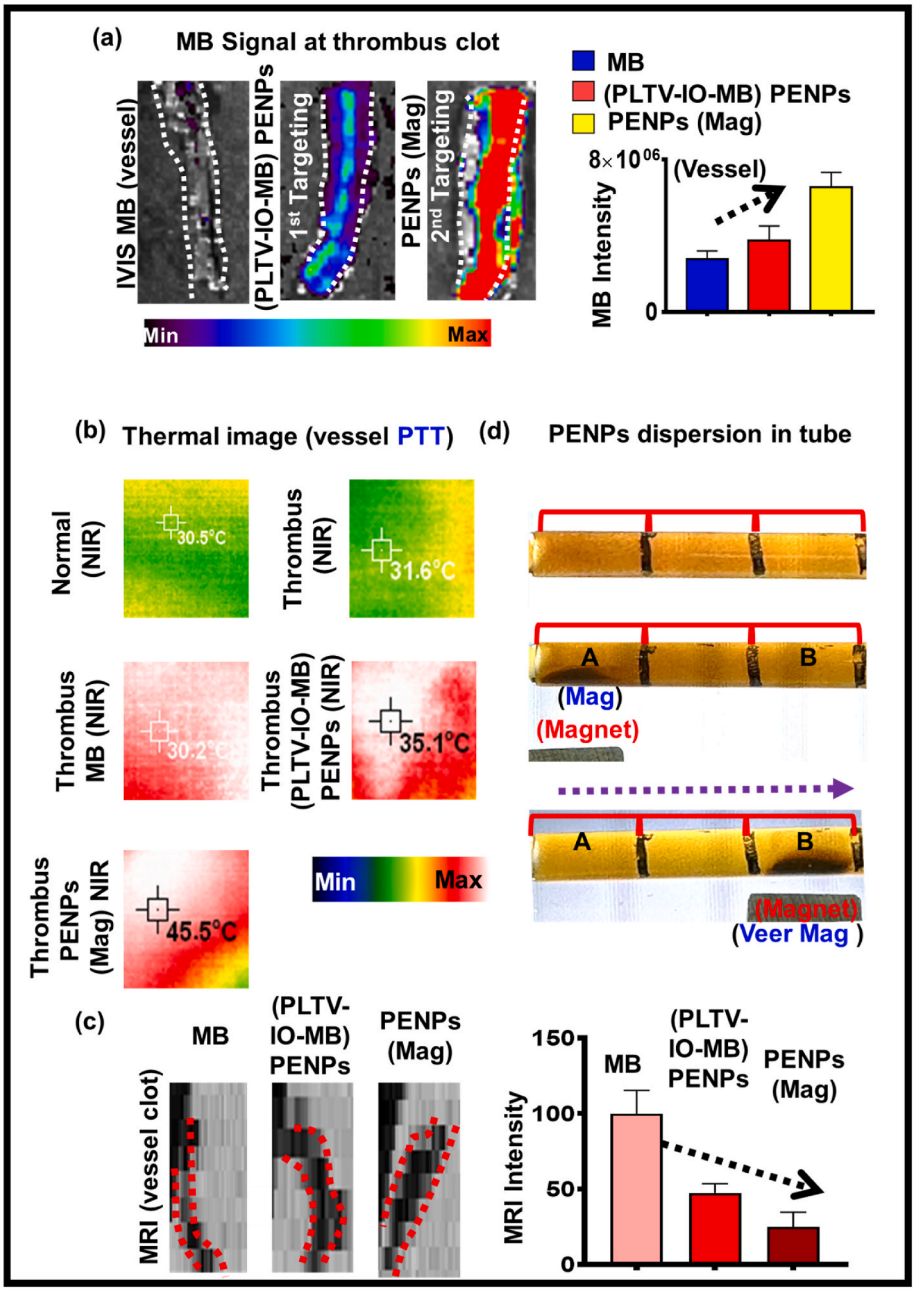

Fig. 5. The results of in vivo theragnostic tests conducted in the study. (a) IVIS, (b) thermal images, and (c) MRI that demonstrate the effectiveness of PLTV–IO–MB PENPs in multimodal thrombus imaging. (d) Photographic data confirmed that capillary tube loading into PLTV–IO–MB PENPs can be magnetically guided to point A under a static magnet for Mag and moved to point B under an actuated magnet for Veer Mag. The experimental data are presented as mean ± standard deviation (SD).

noninvasive methods is still a challenging task. Multimodal biomolecular diagnosing is a potential way to detect thrombi, but noninvasively remote diagnosis and clot lysis remains challenging. In this study, we developed PLTV–IO–MB PENPs that can be used for multimodal imaging. These PLTV–IO–MB PENPs target the IL-6 and P-selectin expressed in thrombus clots, potentially allowing for targeted imaging using IVIS (Fig. 5a), thermal imaging (Fig. 5b), and MRI (Fig. 5c). Animals treated with PLTV–IO–MB PENPs showed higher vascular fluorescent intensities and lower slightly T2 MRI (Fig. 5a, c) at the clot in comparison with the mice treated with MB. However, animals treated with PLTV–IO–MB PENPs and additional static magnetic application had lowest T2 MRI and highest vascular fluorescent intensities at the *ex vivo* clot, indicating that the PLTV–IO–MB PENPs had specifically targeted and penetrated the thrombi. The sensitivity of multimodal imaging were verified (Fig. 5a, b, c), supporting the feasibility of using PLTV–IO–MB PENPs for multimodal thrombus imaging.

Previous studies have shown that photothermal therapy (PTT) can be an effective method for thrombolysis, as it is minimally invasive and has specific spatiotemporal selectivity [75]. Additionally, photosensitizers can be used to aid in ROS-mediated photodynamic therapy (PDT), which causes damage to the peptide bonds of fibrin biological polymeric materials such as N-attached biantennary glycan regions as well as noncovalent interactions [25]. Mechanically magnetic thrombolysis (Veer Mag) has also been proposed as a strategy for thrombolysis [27,76]. Therefore, a combination of PDT, PTT, and Veer Mag could potentially break down the skeleton of fibrin of clot in blood and avoid reembolism. Mice having thrombosis that given treatments of NIR or MB + NIR did not experience significant changes in local temperature (PTT). The temperature for NIR-treated groups were around 30 °C, MB + NIR was around 30 °C, PLTV–IO–MB PENPs was around 35 °C, and PLTV–IO–MB PENPs + Mag was around 45.5 °C (see Fig. 5b).

The photographic result presents the remote positioning of 5 mg of PLTV–IO–MB PENPs in water among a capillary tube, by means of a permanent static magnet for 5 min at a rate of speed (VA) of 0 cm/s, as “Mag” at this step (Fig. 5d). Next, the PLTV–IO–MB PENPs localized were actuated magnetically from position “A" to position “B" alongside the axial tube at a rate of speed (VB) of 1 cm/s, generating a mechanical strength to form veer Mag (magnetotherapy).

3.5. *In vivo studies of thrombolytic efficiency for thrombus animals after administration of phototherapeutic and magnetotherapeutic PLTV–IO–MB PENPs*

To test the safety of the targeted delivery method in vivo, thrombus animals were given PLTV–IO–MB PENPs and their major organs were examined for damage. The results, as shown in Fig. 6a, indicated that there were no signs of inflammatory lesions or organ damage (liver and kidney) in the thrombus animals + Mag + NIR + Veer Mag, thrombus animals + PLTV–IO–MB PENPs + Mag, thrombus animals + PLTV–IO–MB PENPs + Mag + NIR, or thrombus animals + PLTV–IO–MB PENPs + Mag + NIR + Veer Mag, in long-term observation periods, when compared to normal mice. These findings suggest that PLTV–IO–MB PENPs are biocompatible and safe to use. Previous studies have shown that IO-based formulations [77,78] had no obvious toxicity in *in vivo*, which might support our microscopic data.

The effectiveness of the thrombolysis was assessed through a histological evaluation of the thrombosis in vivo (Fig. 6b). The extent of the thrombosis was estimated by determining the percentage of the cross-sectional area of the thrombus clots and vessel. The clot remaining percentages of ca. 92 %, 52 %, 14 %, and 9 % were obtained for thrombus animals + Mag + NIR + Veer Mag, thrombus animals + PLTV–IO–MB PENPs + Mag, thrombus animals + PLTV–IO–MB PENPs + Mag + NIR, or thrombus animals + PLTV–IO–MB PENPs + Mag + NIR + actuated magnetic thrombolysis (Veer Mag) in long-term periods, respectively.

The results indicated long-term treatment with PLTV–IO–MB PENPs, magnetic guidance, and NIR led to a reduced inflammatory response, increased protective effect of HSP, reduced expression of PAI-1, suppressed M1 macrophage, and elevated M2 macrophage, as demonstrated by our histological data (Fig. 6c). Previous studies have also shown that NIR treatment does not cause cytotoxicity or tissue damage when the tissue temperature rises mild-hyperthymia (ca. 45 °C), and it can induce heat shock protein expression for anti-inflammatory purposes [79,80]. Previous research has demonstrated that pre-exposure to heat stress can enhance the survival of ischemic-reperfused skeletal muscles in vivo. This improvement in survival is attributed to the induction of heat shock protein (HSP) expression. The concept of inducing HSP expression for tissue repair is reminiscent of the therapeutic approach of phototherapy [81]. It also found that HSP induced eNOS and thrombomodulin expression and reduced PAI-1 expression [82], where PAI-1 seems to be a risk biofactor for the recurrence and development of cardiovascular thrombotic illnesses [83]. The group treated with PLTV–IO–MB PENPs demonstrated a significant improvement in their ability to convert M1 type macrophages into M2 type macrophages. In vivo experiments further supported this finding by showing that the PLTV–IO–MB PENPs-treated group effectively facilitated the transformation of M2 type macrophages and reduced the M1 type macrophages. Previous published studies have also indicated that photothermal responsive nanoparticles generating mild-hyperthermia can induce the transformation of M1 macrophages into M2 macrophages [84].

Macrophage polarization plays a crucial role in the process of restenosis. Macrophages can be divided into two main polarized types based on the cytokines they secrete and their functions. The first type is the classically activated macrophages (M1 phenotype), which are pro-inflammatory macrophages. The second type is the alternatively activated macrophages (M2 phenotype), which are anti-inflammatory macrophages. In the context of vascular injury, macrophages are polarized towards the M1 phenotype, resulting in the secretion of cytokines that promote proliferation and migration, ultimately leading to restenosis [85]. On the other hand, the M2 phenotype of macrophages has beneficial effects in reducing vascular restenosis. M2 macrophages reduce the secretion of inflammatory cytokines, thereby inhibiting the transformation of smooth muscle cells into a secretory phenotype. They also promote endothelial repair, which reduces inflammatory cell infiltration and inhibits smooth muscle cell proliferation and migration. Additionally, M2 macrophages regulate the proliferation and migration of smooth muscle cells through exosome-mediated mechanisms. Therefore, targeted stimulation of M2 macrophage polarization effectively reduces vascular restenosis [85]. Previously published studies provide evidence for the translation and application of NIR-phototherapeutic techniques in the field of thrombus treatment. Hence, the use of these techniques is anticipated to be feasible and relevant [86–88]. Beside phototherapeutic properties, the developed nanosystem possesses magnetotherapy upon magnetic management for enhancing thrombolytic effectiveness and avoid recurrence of thrombosis.

We further assessed the in vivo therapeutic bioactivity of PLTV–IO–MB PENPs through a mouse liver bleeding assay (Fig. 6d). In this assay, mouse liver were amputated to initiate bleeding 5 min after the administration of MB or PLTV–IO–MB PENPs. The extent of bleeding was used as an indicator to evaluate the risk of hemorrhage. As depicted in Fig. 6d, the normal control group exhibited rapid hemostasis within 5 min, attributed to the inherent hemostatic function in mice. Similar trends in bleeding extent were observed in both the MB-treated group and the PLTV–IO–MB PENPs-treated group. These findings demonstrate that PLTV–IO–MB PENPs, with their outstanding thrombus-targeting capability, exhibit potent thrombolysis activities without posing a risk of hemorrhage in vivo.

The biodistribution of MB and PLTV–IO–MB PENPs were studied in the mice following systemic administration to assess their distribution in physiological conditions. Both formulations were fluorescently evaluated using IVIS in the test animals, and a careful comparison of the two

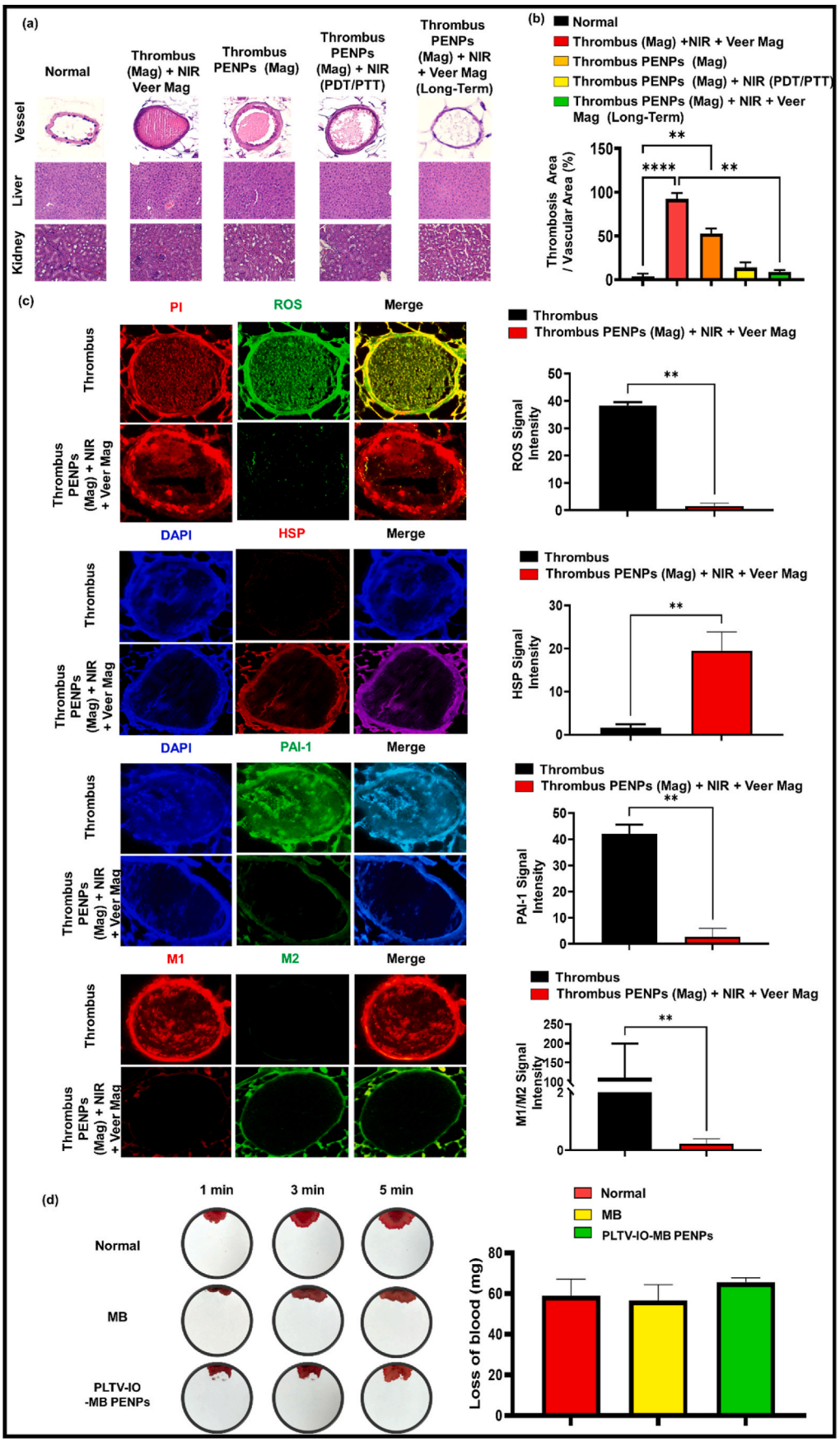

(caption on next page)

Fig. 6. The results of in vivo histological tests conducted in the study. (a) H&E staining of the soft tissues including vessel, liver and kidney. (b) The clot remaining percentage were determined to assess the thrombolysis efficacy. (c) The expressions of biomarkers were fluorescently stained including reactive oxygen species (ROS), heat shock proteins (HSP), plasminogen activator inhibitor-1 (PAI-1) and M1/M2, were evaluated at the site of treated thrombus vessels (using PLTV–IO–MB PENPs + Mag + NIR + Veer Mag) over a long-term period (2 days). This assessment was conducted through biochemical analysis and compared with a group of thrombus-untreated subjects. (d) The in vivo bleeding assays. The experimental data are presented as mean ± standard deviation (SD).

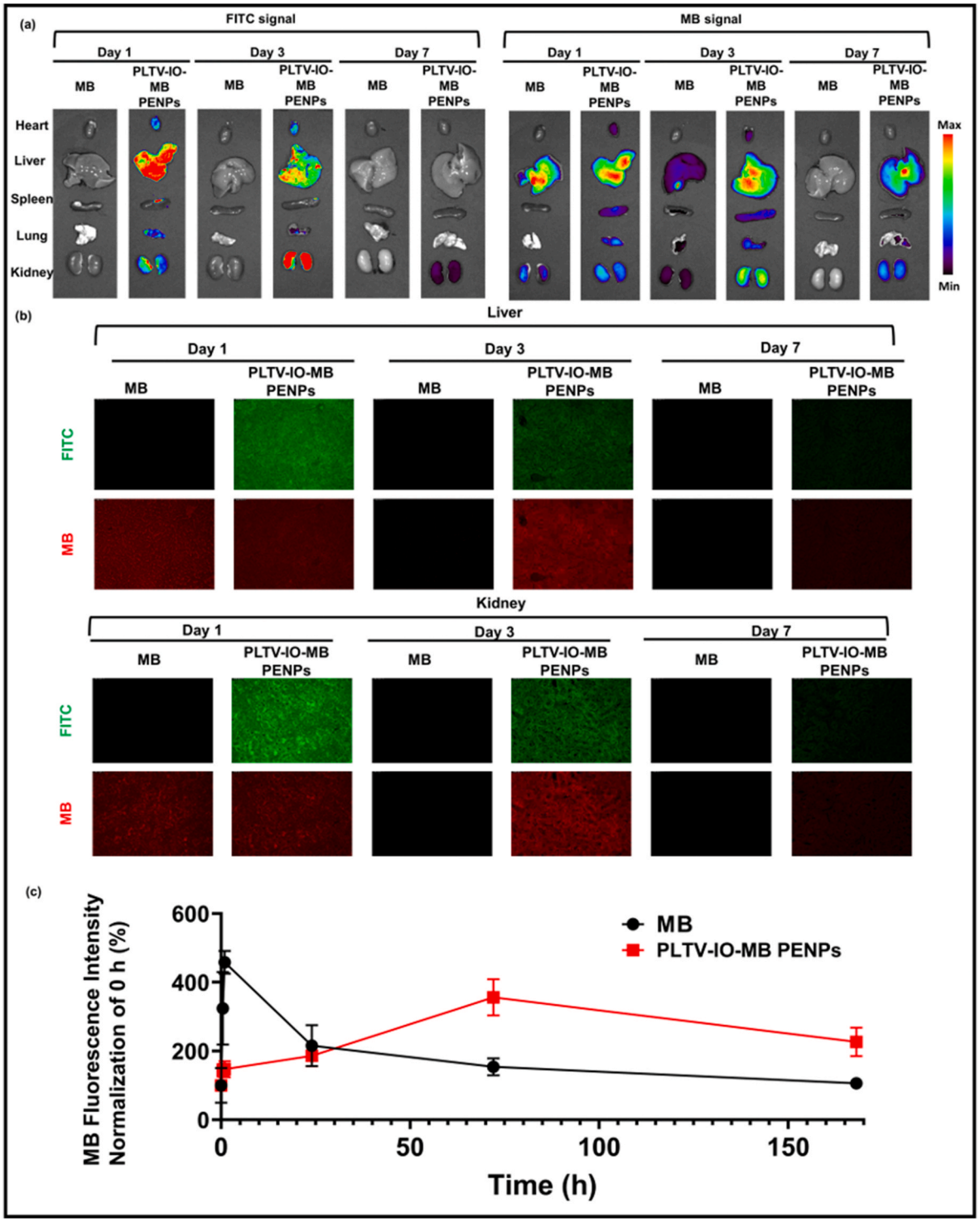

Fig. 7. The findings from in vivo biodistribution tests carried out in this study. The biodistribution data displays the (a) representative organs for IVIS and (b) fluorescent microscopic data, respectively, for mice treated with free-form MB or FITC-conjugated PLTV–IO–MB PENPs. (c) The pharmacokinetic assay. The experimental data are presented as mean ± standard deviation (SD).

formulations was conducted. The fluorescent signals of MB in the organs of the MB-treated group indicated its rapid disappearance over time. In contrast, the signals of MB and FITC associated with PLTV–IO–MB PENPs-treated animals decayed more slowly, confirming the longer presence of the nanocarrier in the body compared to the free-form MB (Fig. 7a). Further assessments using IVIS and microscopic fluorescence imaging validated the reliable data regarding the prolonged effect of PLTV–IO–MB PENPs (Fig. 7a and b).

Fluorescent analysis (Fig. 7a and b) revealed that one day after administration, the fluorescent signals of both free-form MB and PLTV–IO–MB PENPs were detectable in all selected organs. However, at three and seven days after administration, the tissue pattern and intensity of fluorescence from the free-form MB were almost undetectable and significantly reduced compared to the PLTV–IO–MB PENPs group. These findings suggest that both free-form MB and PLTV–IO–MB PENPs formulations can enter the systemic circulation and undergo similar degradation and elimination processes once administered. However, the PLTV–IO–MB PENPs group exhibited slower and longer circulation in the body. This is of great importance in terms of biodistribution, as the stealth properties of PLTV–IO–MB PENPs allow nanomedicine to persist in the body for an extended period in vivo.

The plasma concentration-time curve, as illustrated in Fig. 7c, depicts the pharmacokinetic data following the administration of both free MB and PLTV–IO–MB PENPs. Free MB exhibited rapid elimination from the circulation. In contrast, the incorporation of MB into PLTV–IO–MB PENPs resulted in a significantly improved pharmacokinetic profile. The area under the curve values for MB in PLTV–IO–MB PENPs were several-fold higher than those for free MB. This enhanced pharmacokinetic performance of MB in PLTV–IO–MB PENPs could be attributed to several factors. The hydrophilic polymeric chains of PLTV–IO–MB PENPs might impart a “stealth” property, reducing opsonization and shielding the nanocarriers from elimination. The optimal particle size helps retard renal excretion and recognition by the reticuloendothelial system. In vivo pharmacokinetic investigations in mice corroborate these findings, suggesting that MB encapsulated in PLTV–IO–MB PENPs increases bioavailability and prolongs circulation time.

4. Conclusion

In summary, we developed a potential theranostic PLTV–IO–MB PENPs by combining MB, PLTV, IO, and Pro through a simple self-assembly process under CAP treatment. The functionality of the nanosystem was confirmed through characterization and histological analysis in thrombus animals. The results showed that the nanosystem was specifically accumulated to obstructed vessels, where it exhibited phototherapeutic as well as magnetic sensitivity, resulting in antithrombotic performance. This system has potential for treating various vascular diseases. Despite the promising results of this system, its reliance on external NIR as well as magnetic manipulation presents a challenge for its practical application in settings outside of the hospital, where rapid and safe thrombus lysis is required. However, we remain optimistic that the development of a multimodal technique will soon make biosafe, precise, and thrombus management in home-based healthcare a viable and achievable option.

Ethics approval and consent to participate

This study was approved under the guidelines of the Animal Ethics and Use Committee of Taipei Medical University.

Consent for publication

All of the authors involved in this study have agreed to its publication.

Availability of data and materials

The datasets used in this study are available from the corresponding author upon reasonable request.

Credit author statement

Pei-Ru Jheng: performed in vivo studies and wrote the corresponding parts; Chia-Che Chiang: performed in vivo studies analysis and wrote the corresponding parts; Jiunn-Horng Kang: helped with the design of in vivo studies and wrote the corresponding parts; Yu-Jui Fan: helped with the design of in vivo and wrote the corresponding parts; Kevin C.-W. Wu: helped with the design of material formulation and wrote the corresponding parts; Yan-Ting Chen: performed material analysis and wrote the corresponding parts; Jia-Wei Liang: performed material analysis and wrote the corresponding parts; Nima Bolouki: performed CAP experiments and wrote the corresponding parts; Jyh-Wei Lee: performed CAP experiments and wrote the corresponding parts; Jang-Hsing Hsieh: performed CAP experiments and wrote the corresponding parts; Er-Yuan Chuang: performed material and in vivo experiments and wrote the corresponding parts.

Authors’ information

All authors, including Pei-Ru Jheng, Chia-Che Chiang, Jiunn-Horng Kang, and Yu-Jui Fan who contributed equally to this work, have read, written, and commented on the manuscript and have all agreed to its publication.

Declaration of competing interest

All authors declare that no conflicts of interest exist.

Data availability

The authors do not have permission to share data.

Acknowledgements

This study was financially supported by grants from the National Science and Technology Council (NSTC), Taiwan (111-2320-B-038-039-, 112-2221-E-038-002-MY3 and 112-2622-E-038-006-) and Taipei Medical University Hospital (112TMU-TMUH-01-3). Nima Bolouki acknowledge that he was supported by the project LM2018097, funded by the Ministry of Education, Youth and Sports of the Czech Republic.

References

[1] B. Furie, B.C. Furie, N. Engl. J. Med. 359 (2008) 938–949.
[2] N. Mackman, Nature 451 (2008) 914–918.
[3] B. Li, R. Chen, Y. Zhang, L. Zhao, H. Liang, Y. Yan, H. Tan, D. Nan, H. Jin, Y. Huang, ACS Appl. Bio Mater. 2 (2018) 437–446.
[4] Y. Zhong, Y. Zhang, J. Xu, J. Zhou, J. Liu, M. Ye, L. Zhang, B. Qiao, Z.-g. Wang, H.-t. Ran, ACS Nano 13 (2019) 3387–3403.
[5] Y. Pan, Y. Li, Y. Li, X. Zheng, C. Zou, J. Li, H. Chen, Adv. Healthcare Mater. 12 (2023), e2202281.
[6] Y. Huang, J. Jiang, J. Ren, Y. Guo, Q. Zhao, J. Zhou, Y. Li, R. Chen, Adv. Healthcare Mater. 11 (2022), e2201265.
[7] X. Quan, Y. Han, P. Lu, Y. Ding, Q. Wang, Y. Li, J. Wei, Q. Huang, R. Wang, Y. Zhao, Adv. Healthcare Mater. 11 (2022), e2200416.
[8] Z. Cao, X. Zhang, Z. Wei, C. Song, H. Zou, J. Ran, H. Zhang, D. Xie, S. Han, Y. Wang, Y. Cai, W. Han, J. Nanobiotechnol. 20 (2022) 447.
[9] X. Guo, T. Hong, J. Zang, R. Shao, X. Hou, K. Wang, W. Liu, F. Su, B. He, J. Nanobiotechnol. 20 (2022) 531.
[10] H. Liu, G. Pietersz, K. Peter, X. Wang, J. Nanobiotechnol. 20 (2022) 75.
[11] W. Lv, Y. Liu, S. Li, L. Lv, H. Lu, H. Xin, J. Nanobiotechnol. 20 (2022) 248.
[12] F. Ye, B. Zhang, L. Qiu, Y. Zhang, Y. Zhang, J. Zhang, Q. Zhao, L. Lu, Z. Zhang, Materials today, Bio 16 (2022), 100408.
[13] Y. Ren, H. Jin, X. Ma, Y. Lu, Z. Shen, J. Deng, G.I.N. Waterhouse, S. Guan, Y. Huang, X. Qu, Chem. Eng. J. 455 (2023), 140705.

[14] Y. Wang, L. Lv, H. Liang, W. Liang, Z. Chen, J. Li, S. Liu, F. Hu, J. Zhu, Q. Liu, Z. Wang, Y.-n. Chang, J. Li, M. Li, G. Li, K. Chen, G. Xing, Chem. Eng. J. 441 (2022), 135982.
[15] E.-Y. Chuang, W.-H. Huang, T.-L. Ho, P.-C. Wang, Y.-C. Hsiao, Chem. Eng. J. 429 (2022), 132213.
[16] W.-C. Yan, X.J. Ong, K.T. Pun, D.Y. Tan, V.K. Sharma, Y.W. Tong, C.-H. Wang, Chem. Eng. J. 307 (2017) 168–180.
[17] D. Xu, J. Fan, W. Chen, C. Pan, L. Jiang, D. Kang, W. Li, S. Ding, P. Zheng, B. Hu, M. Zhang, Chem. Eng. J. 446 (2022), 137470.
[18] Z. Wang, M. Li, B. Wang, Y. Xu, J. Li, S. Zhang, Q. Qin, J. Wang, Chem. Eng. J. 451 (2023), 138805.
[19] S.T. Gunawan, K. Kempe, T. Bonnard, J. Cui, K. Alt, L.S. Law, X. Wang, E. Westein, G.K. Such, K. Peter, Adv. Mater. 27 (2015) 5153–5157.
[20] L. Derex, N. Nighoghossian, Nat. Rev. Neurol. 5 (2009) 506–511.
[21] J. Zheng, R. Qi, C. Dai, G. Li, M. Sang, ACS Nano 16 (2022) 2330–2344.
[22] C. Yun, A. Javier, T. Jennings, M. Fisher, S. Hira, S. Peterson, B. Hopkins, N. Reich, G. Strouse, J. Am. Chem. Soc. 127 (2005) 3115–3119.
[23] L.-H. Chang, E.-Y. Chuang, T.-M. Cheng, C. Lin, C.-M. Shih, A.T. Wu, P.-R. Jheng, H.-Y. Lu, C.-C. Shih, F.-L. Mi, Acta Biomater. 134 (2021) 686–701.
[24] T. Burnouf, C.-H. Chen, S.-J. Tan, C.-L. Tseng, K.-Y. Lu, L.-H. Chang, B. Nyambat, S.-C. Huang, P.-R. Jheng, R.N. Aditya, Acta Biomater. 96 (2019) 468–479.
[25] F. Zhang, Y. Liu, J. Lei, S. Wang, X. Ji, H. Liu, Q. Yang, Adv. Sci. 6 (2019), 1901378.
[26] R.T. Li, Y.D. Zhu, W.Y. Li, Y.K. Hou, Y.M. Zou, Y.H. Zhao, Q. Zou, W.H. Zhang, J. X. Chen, J. Nanobiotechnol. 20 (2022) 212.
[27] Q. Deng, L. Zhang, W. Lv, X. Liu, J. Ren, X. Qu, ACS Nano 15 (2021) 6604–6613.
[28] Y.-J. Lu, Y.-H. Wang, R.S. Sahu, J.-P. Chen, B.S. Dash, P.-J. Chung, H.-W. Yang, E.-Y. Chuang, T.-L.J.A.A.M. Hwang, Interfaces 12 (2020) 40141–40152.
[29] Q. Wang, J. Cai, X. Niu, J. Wang, J. Liu, C. Xie, W. Huang, Q. Fan, Biomater. Sci. 9 (2021) 3499–3506.
[30] J. Kim, D. Jo, S.-H. Yang, C.-G. Joo, N. Whiting, S. Pudakalakatti, H. Seo, H.Y. Son, S.-J. Min, P. Bhattacharya, ACS Appl. Mater. Interfaces 13 (2021) 56923–56930.
[31] S.M.M. Moghadam, M. Alibolandi, M. Babaei, J. Mosafer, A.S. Saljooghi, M. Ramezani, J. Biol. Inorg. Chem. 26 (2021) 29–41.
[32] L. Du, W. Chen, J. Zhong, S. Yan, C. Yang, Y. Pu, J. Zhu, T. Chen, X. Zhang, C. Wu, Regen. Biomater. 10 (2023) rbad022.
[33] F. Bertoli, B. Bais, D. De Silvestri, B. Mariotti, D. Veritti, A. Cavarape, C. Catena, P. Lanzetta, L.A. Sechi, G. Colussi, Medicina 57 (2021).
[34] P.T. Wu, C.L. Lin, C.W. Lin, N.C. Chang, W.B. Tsai, J. Yu, Nanomaterials (Basel, Switzerland) (2018) 9.
[35] Y.-H. Chen, E.-Y. Chuang, P.-R. Jheng, P.-C. Hao, J.-H. Hsieh, H.-L. Chen, B. W. Mansel, Y.-Y. Yeh, C.-X. Lu, J.-W. Lee, Mater. Sci. Eng. C 131 (2021), 112488.
[36] N. Bolouki, Y.-N. Hsu, Y.-C. Hsiao, P.-R. Jheng, J.-H. Hsieh, H.-L. Chen, B. W. Mansel, Y.-Y. Yeh, Y.-H. Chen, C.-X. Lu, Int. J. Biol. Macromol. 192 (2021) 506–515.
[37] H.T. Nguyen, N. Bolouki, Y.B. Manga, J.H. Hsieh, E.Y. Chuang, C.H. Chen, Plasma Process. Polym. 17 (2020), 2000110.
[38] M.K. Satapathy, Y.B. Manga, K.K. Ostrikov, W.-H. Chiang, A. Pandey, B. Nyambat, E.-Y. Chuang, C.-H. Chen, ACS Appl. Mater. Interfaces 12 (2019) 86–95.
[39] Y.M. Chen, C.C. Wong, P.W. Weng, C.W. Chiang, P.Y. Lin, P.W. Lee, P.R. Jheng, P. C. Hao, Y.T. Chen, E.C. Cho, E.Y. Chuang, Int. J. Biol. Macromol. 250 (2023), 126105.
[40] Z. He, K. Liu, E. Manaloto, A. Casey, G.P. Cribaro, H.J. Byrne, F. Tian, C. Barcia, G. E. Conway, P.J. Cullen, J.F. Curtin, Sci. Rep. 8 (2018) 5298.
[41] F. Girard-Sahun, P. Lefrançois, V. Badets, S. Arbault, F. Clement, Anal. Chem. 94 (2022) 5555–5565.
[42] C. Hoffmann, C. Berganza, J. Zhang, Med. Gas Res. 3 (2013) 21.
[43] R. Ma, G. Wang, Y. Tian, K. Wang, J. Zhang, J. Fang, J. Hazard Mater. 300 (2015) 643–651.
[44] C.H. Liu, M.C. Liu, P.R. Jheng, J. Yu, Y.J. Fan, J.W. Liang, Y.C. Hsiao, C.W. Chiang, N. Bolouki, J.W. Lee, J.H. Hsieh, B.W. Mansel, Y.T. Chen, H.T. Nguyen, E. Y. Chuang, Adv. Healthc. Mater. (2023), e2301504.
[45] R.F. Marta, N.P. Goette, P.R. Lev, C.D. Chazarreta, C.J. Pirola, F.C. Molinas, Cytokine 29 (2005) 13–17.
[46] M. Saboor, Q. Ayub, S. Ilyas, Moinuddin, Pak. J. Med. Sci. 29 (2013) 891–896.
[47] P.S. Frenette, C.V. Denis, L. Weiss, K. Jurk, S. Subbarao, B. Kehrel, J.H. Hartwig, D. Vestweber, D.D. Wagner, J. Exp. Med. 191 (2000) 1413–1422.
[48] T.-Y. Lu, C.-Y. Chiang, Y.-J. Fan, P.-R. Jheng, E.D. Quinones, K.-T. Liu, S.-H. Kuo, H.Y. Hsieh, C.-L. Tseng, J. Yu, ACS Appl. Mater. Interfaces 13 (2021) 10287–10300.
[49] Y. Zhang, Z. Zhang, R. Wei, X. Miao, S. Sun, G. Liang, C. Chu, L. Zhao, X. Zhu, Q. Guo, B. Wang, X. Li, Arterioscler. Thromb. Vasc. Biol. 40 (2020) 323–334.
[50] C.H. Liu, P.R. Jheng, L. Rethi, C. Godugu, C.Y. Lee, Y.T. Chen, H.T. Nguyen, E. Y. Chuang, J. Nanobiotechnol. 21 (2023) 260.
[51] Y.T. Chen, C.H. Liu, W.Y. Pan, P.R. Jheng, Y.S.Y. Hsieh, T. Burnouf, Y.J. Fan, C. C. Chiang, T.Y. Chen, E.Y. Chuang, ACS Appl. Mater. Interfaces 15 (2023) 32967–32983.
[52] W. Wei, M. Lu, W. Xu, N.E. Polyakov, A.V. Dushkin, W.K. Su, Int. J. Biol. Macromol. 218 (2022) 346–355.
[53] Y.-J. Lu, E.-Y. Chuang, Y.-H. Cheng, T. Anilkumar, H.-A. Chen, J.-P. Chen, Chem. Eng. J. 373 (2019) 720–733.
[54] R. Gitalis, J.H. Bae, M. Preston, M. Patel, Z. Liu, C. Sun, C. Stewart, Y. Xiao, W. L. Siqueira, M. Glogauer, Y. Finer, Acta Biomater. 117 (2020) 283–293.
[55] J. Johnson, Y.W. Wu, C. Blyth, G. Lichtfuss, H. Goubran, T. Burnouf, Trends Biotechnol. 39 (2021) 598–612.
[56] M.A. Rauf, M.A. Meetani, A. Khaleel, A. Ahmed, Chem. Eng. J. 157 (2010) 373–378.
[57] N.V.N. Jyothi, P.M. Prasanna, S.N. Sakarkar, K.S. Prabha, P.S. Ramaiah, G. Srawan, J. Microencapsul. 27 (2010) 187–197.
[58] B. Yuan, H. Wang, J.F. Xu, X. Zhang, ACS Appl. Mater. Interfaces 12 (2020) 26982–26990.
[59] T.T. Nguyen, E.Y. Chuang, Y.P. Chen, P.C. Tseng, M.K. Jhan, C.Y. Lai, Y.T. Wang, Y.P. Hung, C.A. Changou, C.M. Lee, C.L. Chen, C.F. Lin, Biomed. Pharmacother. = Biomed. Pharmacother. 160 (2023), 114397.
[60] M.S. Sivakami, T. Gomathi, J. Venkatesan, H.S. Jeong, S.K. Kim, P.N. Sudha, Int. J. Biol. Macromol. 57 (2013) 204–212.
[61] P. Schubert, Z. Chen, V. Bhakta, B. Culibrk, R. Wambolt, W.P. Sheffield, D. V. Devine, K. McTaggart, Transfusion 61 (Suppl 1) (2021) S131–s143.
[62] M.D. Howard, E.D. Hood, B. Zern, V.V. Shuvaev, T. Grosser, V.R. Muzykantov, Annu. Rev. Pharmacol. Toxicol. 54 (2014) 205–226.
[63] E. Ghasemi, A. Mirhabibi, M. Edrissi, R. Aghababazadeh, R.M. Brydson, J. Nanosci. Nanotechnol. 9 (2009) 4273–4278.
[64] Y. Noishiki, T. Miyata, J. Biomed. Mater. Res. 20 (1986) 337–346.
[65] Z. Han, H. Zhu, J.H. Cheng, ACS Appl. Mater. Interfaces (2023).
[66] D. Pezzoli, E. Cauli, P. Chevallier, S. Farè, D. Mantovani, J. Biomed. Mater. Res. 105 (2017) 2405–2415.
[67] X. Ge, Y. Guo, J. Zhao, J. Zhao, H. Shen, W. Yan, Int. J. Biol. Macromol. 215 (2022) 465–476.
[68] X.R. Ma, X.M. Zhu, J. Li, X. Qi, H.P. Li, J. Tan, Dent. Mater. J. 41 (2022) 473–480.
[69] M. Chu, Y. Shao, J. Peng, X. Dai, H. Li, Q. Wu, D. Shi, Biomaterials 34 (2013) 4078–4088.
[70] S. Sansaloni-Pastor, J. Bouilloux, N. Lange, Pharmaceuticals (Basel, Switzerland) (2019) 12.
[71] H.M. Abdel-Bar, A.A. Walters, J.T. Wang, K.T. Al-Jamal, Adv. Healthcare Mater. 10 (2021), e2001853.
[72] L. Bourré, S. Thibaut, A. Briffaud, N. Rousset, S. Eléouet, Y. Lajat, T. Patrice, J. Photochem. Photobiol., B 67 (2002) 23–31.
[73] N. Ojha, A.S. Dhamoon, Myocardial infarction, StatPearls, in: StatPearls Publishing Copyright © 2023, StatPearls Publishing LLC., Treasure Island (FL), 2023.
[74] A.M. Wendelboe, G.E. Raskob, Circ. Res. 118 (2016) 1340–1347.
[75] Y. Yang, W. Zhu, Z. Dong, Y. Chao, L. Xu, M. Chen, Z. Liu, Adv. Mater. 29 (2017).
[76] Y.H. Ma, S.Y. Wu, T. Wu, Y.J. Chang, M.Y. Hua, J.P. Chen, Biomaterials 30 (2009) 3343–3351.
[77] H. Su, X. Song, J. Li, M.Z. Iqbal, S.S.F. Kenston, Z. Li, A. Wu, M. Ding, J. Zhao, Int. J. Nanomed. 13 (2018) 6987–7001.
[78] C. Ryu, H. Lee, H. Kim, S. Hwang, Y. Hadadian, A. Mohanty, I.K. Park, B. Cho, J. Yoon, J.Y. Lee, Int. J. Nanomed. 17 (2022) 31–44.
[79] Z. Zhao, X. Zhang, H. Zhang, X. Shan, M. Bai, Z. Wang, F. Yang, H. Zhang, Q. Kan, B. Sun, J. Sun, Z. He, C. Luo, Adv. Sci. 9 (2022), e2104264.
[80] W. Yu, N. Yin, Y. Yang, C. Xuan, X. Liu, W. Liu, Z. Zhang, K. Zhang, J. Liu, J. Shi, Acta Biomater. 140 (2022) 625–640.
[81] U. Oron, Photomed. Laser Surg. 24 (2006) 111–120.
[82] T. Uchiyama, H. Atsuta, T. Utsugi, M. Oguri, A. Hasegawa, T. Nakamura, A. Nakai, M. Nakata, I. Maruyama, H. Tomura, F. Okajima, S. Tomono, S. Kawazu, R. Nagai, M. Kurabayashi, Atherosclerosis 190 (2007) 321–329.
[83] K. Yamamoto, K. Takeshita, T. Kojima, J. Takamatsu, H. Saito, Cardiovasc. Res. 66 (2005) 276–285.
[84] X. Chen, X. Zhu, L. Ma, A. Lin, Y. Gong, G. Yuan, J. Liu, Nanoscale 11 (2019) 18209–18223.
[85] F. Li, Z. Rong, R. Zhang, S. Niu, X. Di, L. Ni, C. Liu, iScience 25 (2022), 105147.
[86] P. den Heijer, R.B. van Dijk, M.L. Pentinga, H.L. Hillege, K.I. Lie, J. Intervent. Cardiol. 7 (1994) 525–534.
[87] A. Yadav, A. Gupta, Photodermatol. Photoimmunol. Photomed. 33 (2017) 4–13.
[88] O. Topaz, Cardiology 87 (1996) 384–391.